


**Rebound dynamics of inverse Leidenfrost droplets on dry ice surfaces**Yao-Jun Li <sup>1</sup>, Yi-Zhou Liu <sup>1</sup>, Yi-Bo Wang <sup>2,\*</sup> and Min Chen<sup>1,†</sup><sup>1</sup>*Department of Engineering Mechanics, Tsinghua University, Beijing 100084, China*<sup>2</sup>*Research Center of Engineering Thermophysics, North China Electric Power University, Beijing 102206, China*

(Received 14 May 2024; accepted 7 August 2024; published 3 September 2024)

In this paper, we experimentally investigate the rebound dynamics of droplets on dry ice surfaces, unveiling the mechanism behind the inverse Leidenfrost phenomenon. We demonstrated that the underlying mechanism driving the inverse Leidenfrost phenomenon is the lift force from the air film generated by the sublimation of dry ice. The air film prevents droplet condensation, facilitating the droplet rebound. However, the presence of film significantly depends on impact conditions. During the early spreading stage, bubbles nucleate at the contact line due to the sublimation, then the bubbles grow and gradually form an air film. We showed that the droplet rebound occurs only when the air film fully forms before the maximum spreading stage. Otherwise, the contact line is frozen, ultimately preventing rebound. We propose a theoretical expression of critical air film thickness that determines whether the droplet rebounds. Based on the expression, we ultimately established a theoretical criterion for droplet rebound via thermodynamic and fluid dynamics principles. To validate our developed theoretical criterion, we further investigated the inverse Leidenfrost phenomenon for different fluids, Weber numbers, and different temperatures of droplets. The results demonstrate a high consistency between the predicted results of our theoretical criterion and experimental results.

DOI: [10.1103/PhysRevFluids.9.093601](https://doi.org/10.1103/PhysRevFluids.9.093601)**I. INTRODUCTION**

The impact of droplets on solid surfaces is prevalent in both natural and industrial processes. The behavior exhibited by liquid droplets upon impacting solid surfaces is highly diverse, making it a topic of continual interest within the academic community. Previous studies [1–10] have conducted extensive research on the phenomena following the collision of liquid droplets with solid walls, including the spreading [1–5], the rebound [6,7], the crownlike splashing [8], the fingerlike protrusions [9], the fragmentation [10], and so forth. Among these phenomena, the rebound has drawn great attention in recent years due to industrial needs in areas such as spray cooling [11] and anti-icing [12]. Droplet rebound is a complicated process that is not only influenced by the interaction of inertial, capillary, and viscous forces but also surface features such as wettability, temperature difference between droplet and surface, etc. Some studies [13–21] emphasize that surface wettability is one of the most significant factors because the rebound is only triggered on sufficiently hydrophobic surfaces (a static contact angle greater than  $120^\circ$ ) for isothermal droplets [13]. The rebound mechanism of isothermal droplets on hydrophobic surfaces has been clearly explained through energy analysis methods [14,15]. A droplet usually spreads first after collision and then retracts and rebounds. During the whole process, its kinetic energy is converted

\*Contact author: wybedu54@gmail.com

†Contact author: mchen@tsinghua.edu.cn

into surface tension energy, then back to kinetic energy. However, due to the interaction force between the droplet and the solid surface, part of the energy will always be dissipated, controlled by the wettability, and excessive dissipation caused by hydrophilic surfaces will just prevent the droplet from rebounding. Based on this understanding, previous studies have calculated the remaining kinetic energy of droplets after rebound and established numerous theoretical models for the critical conditions of droplet rebound. The differences among these theoretical models primarily manifest in the simplifying assumptions made during the calculation of viscous dissipation on surfaces with different wetting properties [16–21].

It was mentioned that droplets can rebound on surfaces with sufficient hydrophobicity. In addition, the previous study reported that when the surface temperature is high enough, the rebound can be triggered even on a completely hydrophilic surface [22]. In 1756, Leidenfrost first observed that droplets, when falling onto the surface of an iron pan at 200 °C, could still rebound. This phenomenon was later named the Leidenfrost effect. It should be noted that the occurrence of this phenomenon does not depend on surface wettability; therefore, its rebound mechanism is expected to differ from that of isothermal droplets [23,24]. When a droplet impacts on a hot solid surface, the temperature difference between the droplet and the surface leads to intense evaporation. The generated vapor forms a vapor layer beneath the droplet, preventing direct contact between the droplet and the surface. This vapor layer acts like a cushion, providing pressure for droplet rebound, allowing the droplet to rebound from the solid surface. Hence, the wettability of the surface is no longer the main factor influencing rebound but rather the temperature difference. It has been found that when the surface temperature difference exceeds a certain value, the droplet can generate sufficient vapor and provide enough pressure for rebound [24]. This critical temperature is referred to as the Leidenfrost temperature. It is worth mentioning that the Leidenfrost temperature in essence influences the amount of vapor and its corresponding film thickness. Therefore, existing studies [22–30] denote their efforts to predict vapor layer thickness and develop theoretical models of the Leidenfrost phenomenon. In early studies, it was observed that various factors, such as liquid properties and droplet diameter, influence the phenomenon. For example, Biance *et al.* [22] investigated the variations in the vapor layer corresponding to droplet diameters and their impact on the Leidenfrost temperature and built the model by calculating the conservation of the vapor mass. Cai *et al.* [25] have explored the influence of droplet properties on vapor layer thickness and consequently altered the Leidenfrost temperature by introducing alcohol into the droplets. Although they have found that the Leidenfrost phenomenon can be influenced by several factors and have given several ways to describe the thickness of the film, they did not give an exact expression of the film's shape in theory. To obtain an accurate expression of the film's shape, Burton *et al.* [26] theoretically and experimentally investigated the vapor layer shape of a Leidenfrost droplet. By utilizing optical diffraction methods, they measured the levitating droplets' vapor layer thickness in the Leidenfrost phenomenon at different temperatures. In addition, Tran *et al.* [27] succeeded in measuring the vapor thickness in the spreading process by taking white light with a transparent surface as experiment settings. Based on the studies above, Jiang *et al.* [28] have influenced and controlled the vapor layer by altering the surface structure of the solid walls, guiding steam outward, Mrinal *et al.* [29] made the droplet self-rotate on a ratchet by controlling the flow of vapor below, and Hidalgo-Caballero *et al.* [30] explored the special Leidenfrost state and vapor shape on the cylinder, etc. Overall, current research has provided a relatively clear understanding of the fundamental reasons and influencing factors behind the rebound of liquid droplets on Leidenfrost surfaces.

In comparison to the rebound dynamics on surfaces at room temperature and high temperature, the impact of droplets on cold surfaces has drawn great attention due to the need for anti-icing [12]. However, existing superhydrophobic surfaces can only achieve rebound at temperatures above  $-20\text{ }^{\circ}\text{C}$  [31]. When the surface temperature drops below  $-20\text{ }^{\circ}\text{C}$ , the presence of tiny condensed droplets on the surface disrupts its superhydrophobicity, preventing rebound. Fortunately, a new anti-icing method utilizing surface phase transitions has been developed, enabling droplet rebound even on surfaces with temperatures well below  $-20\text{ }^{\circ}\text{C}$ . Song *et al.* [32] found the occurrence of water droplet levitation on liquid nitrogen surfaces at  $-196\text{ }^{\circ}\text{C}$  and this phenomenon is named

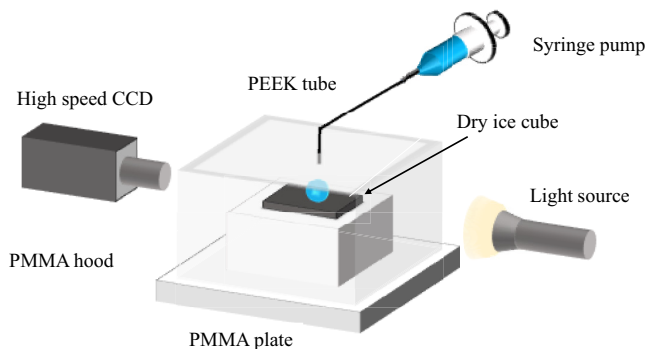


FIG. 1. Sketch of experiment setup. A closed cavity made of PMMA contains an acrylic glass platform for dry ice blocks. A syringe pump connected to a height-adjustable water outlet via a PEEK tube generates liquid droplets of varying sizes by infusing ethanol solutions. Droplet size is controlled by PEEK tube diameter and pump speed, while droplet falling speed is regulated by outlet height.

“inverse Leidenfrost phenomenon” due to its similarity to the Leidenfrost phenomenon, but the mechanism of the inverse Leidenfrost phenomenon is more complex. The factors affecting the inverse Leidenfrost phenomenon contain one more phase change of condensation than those of the Leidenfrost phenomenon so the model of the Leidenfrost phenomenon cannot be directly applied to the inverse Leidenfrost phenomenon. In addition, compared to the extensive research on the Leidenfrost phenomenon, studies on the inverse Leidenfrost phenomenon are currently relatively limited and focus more on the various phenomena. For example, Adda-Bedia *et al.* [33] explored the levitation time of water droplets on liquid nitrogen surfaces and gave a semiempirical expression of the levitation time. Antonini *et al.* [34] explored the spreading factor and rebound time of water droplets falling on dry ice surfaces and gave an empirical formula as well. Milionis *et al.* [35] studied the transport of droplets on dry ice and gave the conditions that allow droplets to remain suspended. Previous studies all demonstrated the phenomenon with the theory that there is an air film beneath the droplet that can lift the droplet. However, they have not explained the formation of the air film or given a mathematical model of the criterion for the occurrence of the inverse Leidenfrost phenomenon.

In this paper, the occurrence conditions of the inverse Leidenfrost phenomenon on dry ice surfaces are investigated. Two objectives are the focus: one is to explore the formation of the air film as well as its influence factors in detail, including the droplet’s radius, velocity, components, and temperature. The other is to develop a theoretical model to predict the occurrence of the inverse Leidenfrost phenomenon.

## II. EXPERIMENTAL SECTION

The experimental setup is illustrated in Fig. 1. A closed cavity was constructed using polymethyl methacrylate (PMMA) material, and within this cavity, an acrylic glass platform was employed to accommodate dry ice blocks. A spirit level was placed on the dry ice surface to ensure approximate horizontal alignment. Positioned at the central upper part of the cavity, there is a height-adjustable water outlet connected to a peristaltic pump via a polyetherketone (PEEK) tube. The pump allows for the infusion of ethanol solutions with varying concentrations. Liquid droplets are generated at the mouth of the PEEK tube and, upon reaching a certain size, are released. The size of the droplets is determined by the diameter of the PEEK tube and the injection speed of the peristaltic pump. In this study, we altered the type of PEEK tube to modify droplet size and adjusted the outlet height to control the droplet falling speed.

Three different types of PEEK tubes were employed, resulting in initial droplet diameters ranging from 0.4 to 2.5 mm and collision velocities between 0.6 and 1.7 m/s. The experiment was recorded using a high-speed camera to capture the entire process of droplet collision with the dry ice surface, enabling the measurement of droplet velocity and size while determining whether rebound occurred. The experiment was conducted at a frame rate of 10 000 frames per second with an exposure time of 1/10 000 s. A lens with a 1 $\times$  magnification rate was used, corresponding to a resolution of 18.425  $\mu\text{m}/\text{pixel}$ . We also heated the reagent in a thermostatic water bath to obtain the desired droplet temperature.

The overall experimental procedure involved placing the high-speed camera at a horizontally focused position, operating the peristaltic pump to release droplets from the PEEK tube's mouth, and continuously altering the ethanol concentration of the droplets to identify the critical composition ratio at which the droplets transition between rebound and adhesion states. Different PEEK tube sizes and droplet falling heights were utilized to explore critical rebound concentrations under varying geometric parameters and velocity conditions. Additionally, we measured the spreading radius and rebound time of droplets of different sizes falling on the dry ice surface using similar experimental steps, providing foundational data for subsequent theoretical calculations. Finally, we change the temperature of droplets to 313 and 333 K and repeat the procedures above. Moreover, variations in temperature during the transfer of liquid from a thermostatic water bath to the syringe pump can result in discrepancies between the intended and the actual droplet temperatures. To mitigate this, we maintain the temperature of the bath at 318 and 338 K, which are 5 $^\circ$  higher than our target temperature, thus compensating for potential heat loss during the experiment.

### III. RESULTS AND DISCUSSION

As mentioned above, droplet rebound will be influenced by the interaction of inertial, capillary, and viscous forces and surface features such as wettability, temperature difference between droplet and surface, etc. To get a more general comprehension of the inverse Leidenfrost phenomenon, we first conduct the experiment with water droplets within Weber numbers ranging from 0 to 100. To verify the rationality, we make a quantitative comparison with the results of Antonini *et al.* [34]. The range of Weber numbers is limited due to the size and the velocity of the droplet, since it is hard to get a very large liquid droplet, and the droplet will always break up if the velocity is too high so that we cannot observe the rebound of droplets. We examined the effect of Weber numbers and measured the spreading coefficient and rebound time of water droplets in the inverse Leidenfrost phenomenon. The result is shown in Appendices A and B. Then we change the property of droplets by adding alcohol to see its effect. Given that alcohol is a typical low-viscosity fluid, it is expected to exhibit similar dynamic characteristics to water within the Weber number range of 0–100. When we use alcohol droplets as experimental objects, we observe a transition from droplet rebound to nonrebound for ethanol-water mixtures when the ethanol concentration exceeds a certain threshold. This phenomenon is illustrated in Fig. 2. Image (a) depicts the process of a typical water droplet falling onto a dry ice surface, illustrating the stages of contact, spreading, retraction, and rebound. This phenomenon aligns with the experimental observations of Antonini *et al.* [34]. In contrast, images (b) and (c) showcase alcohol droplets of the same size and velocity but with varying concentrations. While their spreading processes mirror those of water droplets, during the final stage of retraction, the 57% concentration droplet completely detaches from the surface and rebounds, whereas the 60% concentration droplet does not. Simultaneously, we observe that when droplets fail to rebound, the contact diameter during the retraction process is significantly larger than in the previous two scenarios. This may be attributed to the freezing adhesion of the droplet's bottom surface to the dry ice surface. In addition, we find that water droplets can always rebound at any Weber number within the range of our experiment but alcohol droplets can only rebound in certain situations. This phenomenon has not been documented in prior research.

Based on the findings above, we seek to explain this occurrence through the lens of existing theoretical frameworks. Adopting a classical model primarily employed in the context of the Leidenfrost

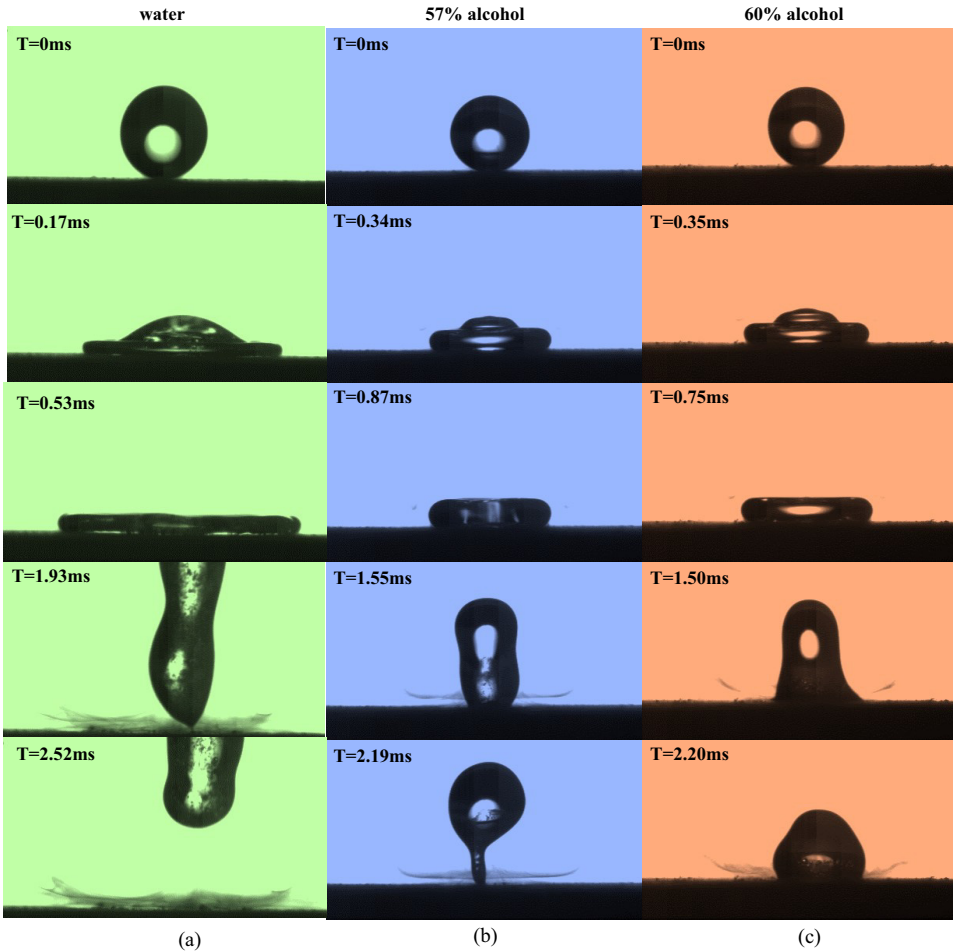


FIG. 2. Snapshots of a water droplet (a), a water droplet with 57% (b), and a water droplet with 60% (c) alcohol impact dry ice surfaces. The black shadow near the impact site represents condensed water vapor, as documented in prior scholarly research, without compromising our investigation into droplet dynamics on dry ice.

phenomenon [25], which exhibits a semblance to the performance observed in our experiment, they utilize the vapor layer thickness as a crucial criterion for assessing the necessity of elevating the surface temperature. So we take the thickness to judge whether the drop rebounds. The outcomes of their analysis are depicted in Fig. 3, which shows that this model is not suitable for our study. Here we define the thickness of the air film as  $\delta$  ( $\delta$  only represents the thickness in Fig. 3; the thickness of the air film will be discussed again in the following text). The critical condition proposed by Milionis *et al.* [35] cannot perfectly judge the suspension of alcohol droplets, either. Additionally, we explore an alternative approach by employing the methodologies commonly applied to superhydrophobic surfaces to explicate our phenomenon. However, the prescribed criterion employed in conventional superhydrophobic models proves impractical for direct application to our experimental conditions, thereby precluding the utilization of their model to comprehensively characterize our experimental outcomes.

In detail, in the Leidenfrost phenomenon, the substantial temperature difference ensures rapid evaporation of the portion of the droplet in initial contact during the collision, leading to prompt

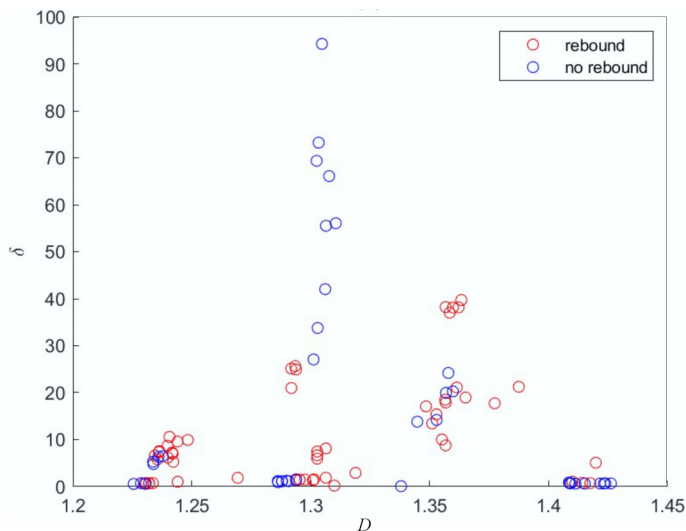


FIG. 3. Comparison of predicted results utilizing the Leidenfrost phenomenon model with our experiment results [25].  $D$  is the diameter and  $\delta$  is the thickness of the film. No discernible difference in was observed between rebound and nonrebound cases, contrary to the model's predictions.

separation from the surface. However, in our experiment, even when the substrate temperature is adequately low, drops struggle to rebound as they may freeze and adhere to the surface (see details in Appendix C). Therefore, the Leidenfrost model appears to differ significantly from our experimental findings. Similarly, the superhydrophobic surfaces model, which considers viscous dissipation due to different contact angles, does not apply to our experiment, where liquid drops have difficulty remaining on dry ice, precluding the measurement of their contact angles. In summary, a new model is required to elucidate the condition of the inversed Leidenfrost phenomenon on dry ice substrates in our experimental setup.

To explain the rebound condition, we model the droplet's rebound process (as shown in Fig. 4, illustrating the spreading and rebound process of the droplet, and marking the parameters needed for the model). Unlike typical semiempirical models that establish models based on energy relationships, we consider the forces acting on the droplet during the rebound process. First, to calculate the force and the radius of the droplet, we simplify the droplet impact process to a uniformly spreading liquid sphere on a uniform air film. It is admitted that the bottom of the droplet when collision is not uniform. However, here we simplify the bottom as a plain surface. Therefore, the height of the

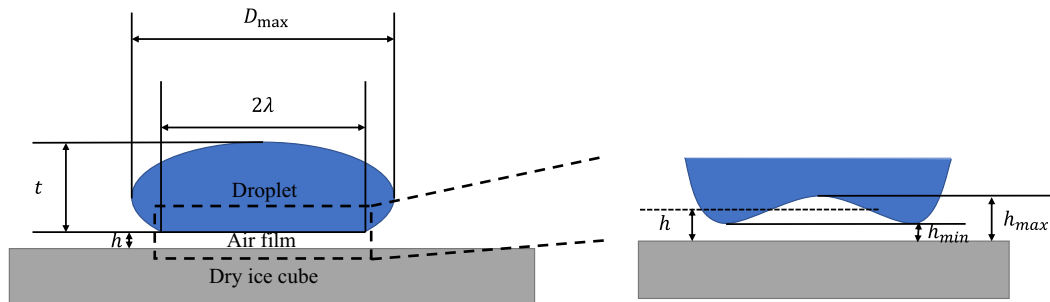


FIG. 4. The schematic depiction of the theoretical model: the ideal model constructed on the left, and the actual shape of the gas film at the droplet's base on the right.



air film thickness can be regarded as an average height, and the specific effect of the bottom's shape will be discussed below.

When the droplet reaches its maximum spreading diameter, the thickness of the air film below reaches its minimum. At this point, the mass of carbon dioxide within the air film no longer changes. Therefore, the amount of carbon dioxide generated by the sublimation of dry ice below is exactly equal to the sum of the amount absorbed by the droplet and the amount expelled outward by the air film. This approach of considering gas mass conservation is also employed in related studies on the Leidenfrost phenomenon [22]. Therefore, we can calculate these three amounts of carbon dioxide and establish an equation [see Eq. (4)]. Let the thermal conductivity coefficient of carbon dioxide be  $k$ , the latent heat of sublimation of dry ice be  $L$ , the thickness of the air film be  $h$ , the temperature difference between dry ice and the droplet be  $\Delta T$ , and the radius of the droplet spreading be  $\lambda$ . We can then write the equation for the carbon dioxide generated due to sublimation as follows:

$$\frac{dm}{dt} = \frac{k\Delta T}{Lh}\pi\lambda^2. \quad (1)$$

However, since the droplet itself absorbs carbon dioxide, we initially employ the simple Fick's law for calculation (we will explain the reason for choosing this model later). Let the diffusion coefficient be  $D$ , and the gas density be  $\rho_v$ :

$$\frac{dm}{dt} = -\pi D\lambda^2 \frac{\rho_v}{h}. \quad (2)$$

When the air film is stably present, it will flow outward in a Poiseuille flow manner. Let the gas viscosity coefficient be  $\eta$ , and the pressure difference between the center of the air film and the external pressure be  $\Delta P$ . This can be expressed as

$$\frac{dm}{dt} = -\rho_v \Delta P \frac{2\pi h^3}{3\eta}. \quad (3)$$

The overall equilibrium equation for the conservation of mass is given by

$$\frac{k\Delta T}{Lh}\pi\lambda^2 - \pi D\lambda^2 \frac{\rho_v}{h} - \rho_v \Delta P \frac{2\pi h^3}{3\eta} = \frac{dm}{dt} = \frac{d}{dt}(\rho\pi\lambda^2 h). \quad (4a)$$

From the analysis above, in the right part of the equation, we have  $\dot{\lambda} = 0$  and  $\dot{h} = 0$ , so the right part is just 0 when the droplet reaches its maximum spreading diameter. So we get

$$\frac{k\Delta T}{Lh}\pi\lambda^2 - \pi D\lambda^2 \frac{\rho_v}{h} - \rho_v \Delta P \frac{2\pi h^3}{3\eta} = 0. \quad (4b)$$

We know that when  $We < 10^1$ , the spreading radius  $\lambda \propto R We^{1/2}$ , and when  $We > 10^1$ , it follows  $\lambda \propto R We^{1/4}$ , where  $R$  is the initial radius of the droplet and the conclusion is still valid at different liquid temperatures (see Appendix A for derivation). Regarding the term  $\Delta P$  in the Poiseuille flow formula, we consider two sources: (1) the gravity of the droplet itself,  $\frac{4}{3}\pi R^3 \rho g$ ; and (2) the change in momentum of the droplet during spreading. We average this momentum change over the entire spreading process to calculate the second part of the pressure,  $\frac{mv}{0.5\tau\pi\lambda^2}$ , where  $v$  is the velocity before droplet impact and  $\tau$  is the rebound time obtained in Appendix B. The time from impact to maximum spreading is the same as the time for the final retraction according to the water spring model, so we take half of the rebound time as the spreading time. (In fact, the scale factor has little effect on the final result.) The droplet mass is  $m = \frac{4}{3}\pi R^3 \rho$ , and we use a linear mixture approach for droplet

density. So the expression of  $\Delta P$  is  $\Delta P = \frac{mg + \frac{mv}{0.5\tau}}{\pi\lambda^2} = \frac{\frac{4}{3}\pi R^3 \rho g + \frac{4}{3}\pi R^3 \rho v}{\pi\lambda^2} = \frac{R We^{1/2}}{\rho g} \left( \frac{4}{3} + 1.026 \frac{\sqrt{We}}{Bo} \right)$ . Substituting these values, we obtain the relationship for the droplet thickness  $e$  when the droplet

spreads to its maximum diameter:

$$h^4 \propto \frac{\eta}{\rho_v \Delta P} \lambda^2 \left( \frac{k \Delta T}{L} - D \rho_v \right). \quad (5)$$

Now, let us consider the expression inside the parentheses. We first explain here the reason for using Eq. (2) in this form. We consider several possibilities regarding the interaction between carbon dioxide and the droplet including chemical interaction, absorption by diffusion, absorption by internal flow in the droplet, and absorption due to the breakup of the droplet. However, there is no violent chemical interaction between water, ethanol, and carbon dioxide. Additionally, although other interactions may occur after the droplet breaks, the droplet does not break during the spreading process in our scenario. Thus, we only need to account for the absorption of carbon dioxide. By looking up the diffusion coefficients of carbon dioxide in water and ethanol, we find that regardless of the mixing ratio, the order of magnitude of the term on the right side of the parentheses remains around  $10^{-10}$ , while the left side is on the order of  $10^{-3}$ . Even if we consider the enhanced diffusion absorption effect of the internal flow in the droplet [36], the right side remains significantly smaller than the left side. Therefore, the effect of the right side can be neglected. Substituting  $We = \frac{\rho v^2 R}{\sigma}$ ,  $Bo = \frac{\rho g R^2}{\sigma}$  into the expressions for  $\Delta P$  and  $\lambda$ , we get

$$h^4 \propto \frac{\eta k \Delta T R}{\rho_v L \rho g} \frac{We^{4i}}{\frac{4}{3} + 1.026 \frac{\sqrt{We}}{Bo}}, \quad (6)$$

where  $i = \begin{cases} 1/2, & We < 10 \\ 1/4, & We > 10 \end{cases}$ .

In the inverse Leidenfrost phenomenon, the rebound of droplets is not only influenced by the sublimation of the underlying dry ice but also by the freezing of the droplets themselves in low-temperature conditions. If the droplet wants to retract and rebound after complete spreading, its proximity to the dry ice must be limited to prevent condensation which can increase kinetic energy losses and hinder the droplet from retracting and rebounding. The effect of contact can be roughly estimated. Taking unsteady state heat conduction theory, it can be easily found that the heat transfer efficiency in direct contact between the solid and liquid is hundreds of times greater than the case where there is an intermediate gas layer. More specifically, if we compute the heat transfer in the rebound process, it can be verified that the temperature of the bottom can indeed reach the ice point. (The specific calculation process is detailed in Appendix C, and the rule is also valid at different liquid temperatures). Moreover, experiments conducted by Schremb *et al.* [37] and Jin *et al.* [38] have already proved that when water droplets come into contact or collide with cold substrates, they can readily nucleate, freeze, and ultimately adhere to the surface. More specifically, the whole collision process is illustrated in Fig. 5. Upon initial contact with the substrate, the droplet triggers the emergence of bubbles at the point of contact, a result of sublimation. As the droplet spreads across the surface, these bubbles concurrently expand. Upon reaching its maximum radius, if the bubbles attain a critical size, they can form an air film and lift the droplet from the surface, facilitating its rebound. However, should the bubbles fail to reach the requisite size, they are unable to lift the droplet, resulting in continuous contact between the droplet's periphery and the dry ice surface. Ultimately, this persistent contact leads to condensation, thereby precluding the droplet from rebounding. A similar process has been found in the Leidenfrost phenomenon [39].

The thickness we get is from an idealized uniform shape, while the exact shape of the bottom air film (regardless of whether it is a bubble or an air film) is shown in Fig. 4, where the neck part of the bottom is noticeably thinner. Therefore, we believe that at the maximum spreading, the calculated thickness of the air film beneath the droplet needs to exceed a certain value to keep the whole droplet away from the dry ice surface. When the air film thickness is greater than this value, the condensation dissipation from the droplet itself will not significantly affect the rebound. However, when it falls below this value, the condensation dissipation from the droplet cannot be ignored, leading to the droplet's inability to rebound. Once we identify this critical thickness, we



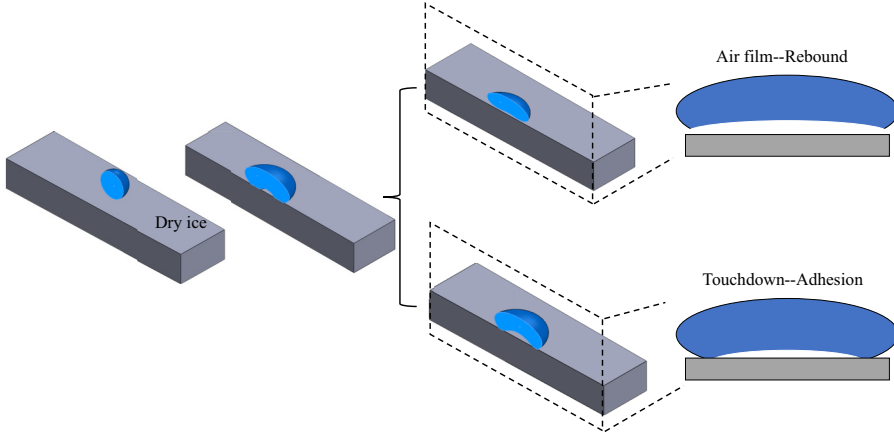


FIG. 5. The different results after droplets impact on the dry ice surface. When bubbles successfully form a film, droplets can rebound. Otherwise, droplets can only adhere to the surface.

can calculate and determine whether the droplet can rebound based on its own parameters. We denote this critical thickness as  $h_0$ . The critical condition for droplet rebound is then expressed as

$$h_0^4 \propto \frac{\eta k \Delta T R}{\rho_v L \rho g} \frac{We^{4i}}{\frac{4}{3} + 1.026 \frac{\sqrt{We}}{Bo}}, \quad (7)$$

where  $i = \begin{cases} 1/2, & We < 10 \\ 1/4, & We > 10 \end{cases}$ . We express this critical relationship in a different form:

$$\frac{\rho_v L \rho g h_0^4}{\eta k \Delta T R} \propto \frac{We^{4i}}{\frac{4}{3} + 1.026 \frac{\sqrt{We}}{Bo}}. \quad (8)$$

At this point, both ends are dimensionless, where  $\rho_v = 1.122 \text{ kg/m}^3$ ,  $L = 0.709 \text{ kJ/mol}$ ,  $\eta = 10.9 \times 10^{-6} \text{ Pa s}$ ,  $k = 0.0139 \text{ J/m s K}$ , and in this experiment,  $\Delta T = 98 \text{ K}$ . Let the ethanol proportion in the solution be denoted by  $x$ ; then the density  $\rho = 1 - 0.21x \text{ g/cm}^3$  and the surface tension coefficient are obtained by looking up tables [40] and linear interpolation. The proportionality coefficient and the critical thickness  $h_0$  can be obtained through experimental fitting, and we have found that when  $h_0 \propto R^{1/4}$ , there will be a best fitting result.

Consequently, we obtain a dimensionless number—the inverse Leidenfrost number  $IL = \frac{\rho_v L \rho g h_0^4}{\eta k \Delta T R}$  and there is a critical  $IL$  number  $IL_c$  to judge whether droplets can rebound. By making both sides dimensionless, we experimentally plot the relationship between the critical  $IL$  number  $IL_c$  and the Combining number  $= \frac{We^{4i}}{\frac{4}{3} + 0.513 \frac{\sqrt{We}}{Bo}}$ , resulting in Fig. 6(a).

From the figure, it is evident that the critical thickness is solely associated with the critical number  $IL_c$ , such as density  $\rho$ , temperature difference  $\Delta T$ , and radius  $R$ , with no dependency on velocity  $v$ , as  $IL_c \propto \frac{\rho h_0^4}{R \Delta T}$ . This observation that velocity is independent can be explained by considering the dynamic characteristics of the air film beneath the droplet. The air film's thickness is determined by pressure and radius, where higher pressure and a larger droplet lead to a thicker air film [23]. Since the air film is generated by dry ice, a greater temperature difference results in increased gas production, subsequently raising the pressure. The pressure primarily originates from gravity force and inertia force. The relationship between gravity force, density, and radius is straightforward. However, for inertia force, a novel conclusion emerges—the pressure is independent of velocity. Initially, if the droplet's Weber number ( $We$ ) is less than 10, the inertia force can be disregarded due to its insignificance. As the Weber number becomes sufficiently large, we can calculate the

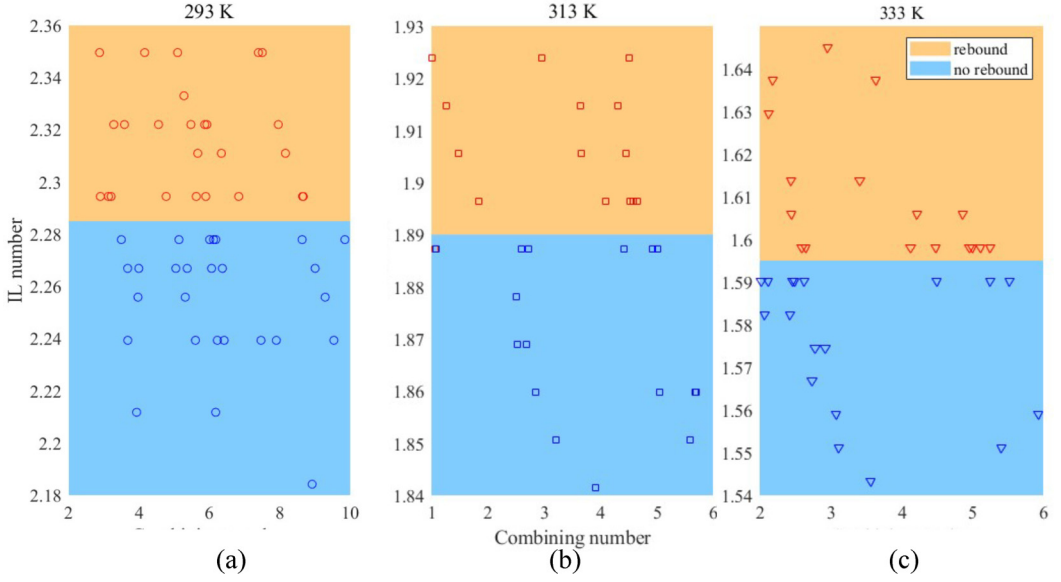


FIG. 6. Comparison of theory and experiment results. A clear boundary delineates the relationship between the final critical  $IL_c$  number and the combining number. Red points signify rebounded droplets, while blue points indicate adhered droplets. The figures show experiment results at different liquid temperatures and the corresponding critical number  $IL_c$  is just inversely proportional to  $\Delta T$ :  $IL_c \propto \frac{1}{\Delta T}$ .

pressure by

$$P = \frac{mv}{\tau \pi \lambda^2}. \quad (9)$$

Based on the previous findings, we observe that  $\lambda \propto R We^{1/2}$ , and the spreading time  $\tau$  exhibits no correlation with velocity. Upon incorporating the expression  $We = \frac{\rho v^2 R}{\sigma}$  into the equation, we note that the pressure miraculously remains unaffected by velocity. Therefore, we confidently assert that the critical thickness is independent of velocity, aligning perfectly with the outcomes of our experimental study.

The preceding discussion has addressed the influence of velocity, density, and radius on the phenomenon under consideration. Now, we extend our analysis to incorporate temperature as a contributing factor. We change the temperature of the liquid and explore the rebound situation at 313 and 333 K, respectively. The experimental findings at three different temperature conditions are graphically depicted in Fig. 6, revealing the presence of a discernible critical number  $IL_c$  dictating the droplet rebound outcome. Specifically, the critical numbers  $IL_c$  at different temperatures are 2.29 (a), 1.89 (b), and 1.59 (c), respectively. Notably, these values exhibit a proportional relationship mirroring the temperature differences. We theoretically explore the linkage between the temperature difference and the critical number  $IL_c$ . The air beneath droplets comes solely from dry ice sublimation, so its weight and density depend directly on how quickly heat moves. Leveraging Fourier's law of heat transfer, it is discerned that density exhibits a direct correlation with temperature differential  $\rho \propto m = \int \frac{k \Delta T}{Lh} \pi \lambda^2 dt \propto \Delta T$ . Additionally, the air pressure within the droplet's vicinity is intrinsically linked to the temperature disparity  $P = \rho RT \propto \Delta T$ . Drawing from Burton's [26] seminal work, it is ascertained that the altitude discrepancy between the thinnest and thickest regions of the air film is positively associated with pressure gradients  $\Delta h \propto P \propto \Delta T$ . Typically, we assume an air layer forms when it is thicker than half the height difference mentioned earlier. Hence, the critical thickness we suggest depends on that height difference, which is related to how

much the temperature varies,  $h_0 = \frac{1}{2} \Delta h \propto \Delta T$ . And this relationship just fit the expression of the  $IL_c$  number. In culmination, our analysis corroborates a positive correlation between the critical thickness and temperature difference, thereby corroborating the empirical observations derived from our experimental endeavors.

#### IV. CONCLUSION

In this paper, we experimentally investigated the rebound phenomenon of droplets' impact on the dry ice surfaces. We explained the formation process of the air film and developed a criterion of the occurrence of the inverse Leidenfrost phenomenon. We found that the air film is converged with the bubbles generated by dry ice, only when enough bubbles can form a completed air film. The rebound criterion is mainly decided by the formation of the air film beneath the droplet. We took the air film thickness to display the degree of completion and proposed a critical thickness. By considering the mass conservation of air, we calculated a dimensionless thickness  $IL$  number and a dimensionless critical thickness  $IL_c$ . If the  $IL$  number of the droplet is bigger than  $IL_c$ , then the droplet can rebound. Moreover, we have explored the influence factor of the critical number  $IL_c$  and found that it is solely influenced by the density, radius, and temperature disparity between the droplet and substrate, with no discernible correlation to its velocity.

#### ACKNOWLEDGMENTS

We are grateful to Yang Liu for his help in experiments. This work is supported by the National Natural Science Foundation of China (Grants No. 11972211, No. 52306134), the Natural Science Foundation of Hebei Province of China (Grant No. E2023502027), and the National College Students Innovation and Entrepreneurship Training Program in China (Grant No. 202310003055).

#### APPENDIX A: THE MAXIMUM SPREADING DIAMETER

Before a droplet undergoes rebound, it must first experience spreading and then recoiling, ultimately leading to rebound. The characteristics of droplet spreading during this process will significantly influence the subsequent rebound dynamics. Therefore, before investigating the rebound dynamics of droplets, it is essential to explore the dynamic characteristics of droplets during the spreading and recoiling stages.

Given the crucial impact of droplet spreading diameter and contact time on heat transfer, we have investigated the maximum spreading diameter of droplets during the spreading process, along with the overall duration from spreading to recoiling and rebound.

We initially measured the maximum spreading diameter of droplets (Fig. 7 presents the experimental setup for measuring the spreading diameter), and compared it with the results of droplets on superhydrophobic surfaces and the droplet spreading results on dry ice surfaces conducted by Antonini *et al.* [34] (depicted in experimental data shown in Fig. 8). Our experimental data exhibits a close resemblance to previous measurements on dry ice when the Weber number exceeds 10. However, a noticeable deviation from the patterns proposed by previous studies is evident when  $We$  is less than 10. It is apparent that the physical model explaining the maximum spreading coefficient of droplets in this range differs from conventional research. Furthermore, we conducted a detailed exploration of the physical laws governing the maximum spreading coefficient of droplets on dry ice surfaces.

In the range where the Weber number exceeds 10, following the theory of Clanet *et al.* [1], during the rebound process, the collision time  $\tau$  is proportional to  $\tau \propto \frac{D_0}{v}$ , and the acceleration  $a$  is proportional to  $a \propto \frac{v^2}{D_0} \gg g$ . Therefore, it can be considered an enhanced gravitational field. In this enhanced gravity field, the capillary length, originally denoted as  $a \equiv \sqrt{\frac{\sigma}{\rho g}}$ , now changes to

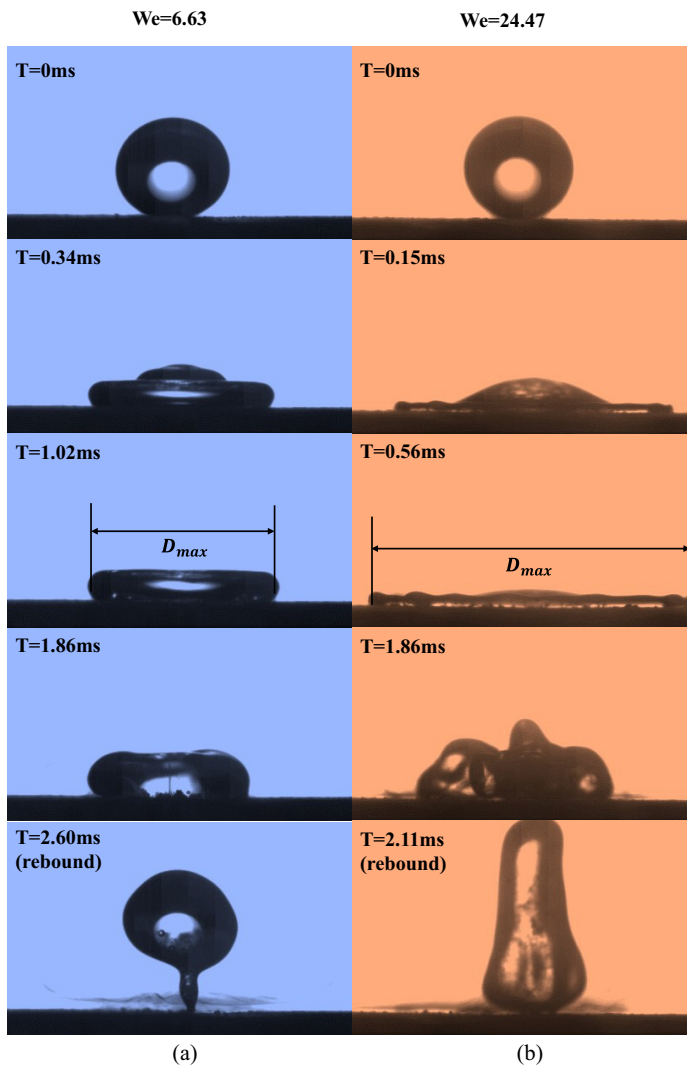


FIG. 7. The whole process of the rebound for droplets in different  $We$  numbers is shown in the figure. The maximal spreading diameter and the rebound time are defined in the figure.

$a = \sqrt{\frac{\sigma}{\rho a}}$ . By incorporating volume conservation, we can derive the following:

$$D_{\max} \propto D_0 We^{1/4}. \quad (\text{A1})$$

Before deriving this conclusion, we did not consider any properties of the underlying surface, whether it is superhydrophobic or dry ice. The observed pattern of the maximum spreading coefficient for droplets applies to this derivation, and our experiments indeed confirm the generality of this theory within this Weber number ( $We$ ) range.

However, in the  $We > 10$  range, the maximum spreading coefficient of droplets exhibits a distinct pattern, which was not observed in the study by Antonini *et al.* [34]. Recently, Liu *et al.* [41] investigated the maximum spreading pattern of droplets on superhydrophobic surfaces within the  $We < 10$  range. Based on their research, we theoretically model the maximum spreading coefficient of droplets on dry ice in our experiments within the  $We < 10$  range.

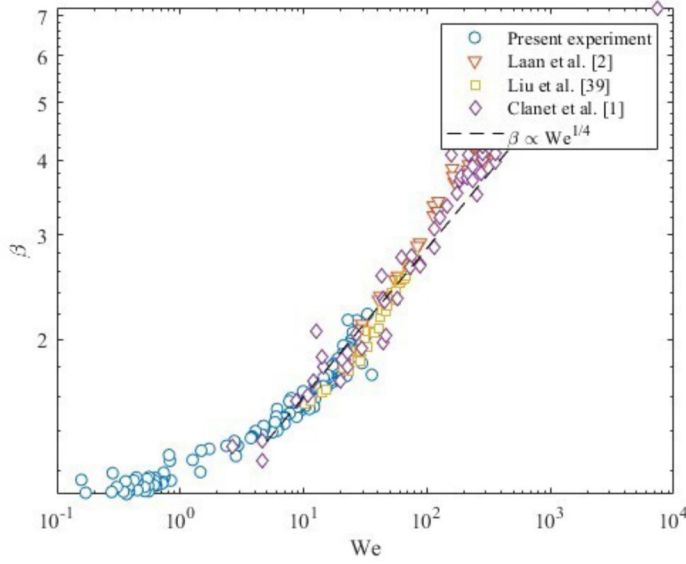


FIG. 8. Our experiment results are compared with those of former researchers in this figure. It shows that our results are aligned with theirs when the We number is bigger than 10, while not aligned when the We number is smaller than 10.

Within the  $We < 10$  range, it is reasonable to assume that the droplet achieves maximum spreading in an ellipsoidal shape. Let the equatorial radius of the ellipsoidal droplet be denoted as  $a$ , and the polar radius as  $b$ . Based on the conservation of droplet mass, we have

$$m = \frac{1}{6}\pi D_0^3 \rho = \frac{4}{3}\pi a^2 b \rho. \quad (\text{A2})$$

Based on the conservation of energy, we have

$$E_{ki} + E_{pi} + E_{Si} = E_{pf} + E_{Sf}. \quad (\text{A3})$$

The subscripts  $i$  represent the moment just before the collision,  $f$  denotes the instant of maximum spreading, and the subscripts  $k$ ,  $p$ , and  $S$  represent the kinetic energy term, gravitational potential energy term (with the collision surface as the zero point), and surface energy term, respectively. The initial state is defined as

$$E_{ki} = \frac{1}{2}mv^2, \quad E_{pi} = \frac{1}{2}mgD_0, \quad E_{Si} = \gamma\pi D_0^2. \quad (\text{A4})$$

The energy state at the moment of maximum spreading is defined as

$$E_{pf} = mga, \quad E_{Sf} = \gamma\left[\frac{4}{3}\pi(a^2 + 2ab)\right]. \quad (\text{A5})$$

Then we can get

$$We + Bo + 12 = \frac{1}{4}Bo\frac{D_0^2}{a^2} + 16\frac{a^2}{D_0^2} + 4\frac{D_0}{a}. \quad (\text{A6})$$

Here,  $We = \frac{\rho D_0 v^2}{\sigma}$  and  $Bo = \frac{\rho g D_0^2}{\sigma}$  have already been used. Directly solving for  $a$  is rather challenging; therefore, let us first consider two special cases: When  $Bo = 0$ , i.e.,  $g = 0$  (neglecting gravity), we have

$$We + 12 = 16\frac{a^2}{D_0^2} + 4\frac{D_0}{a}. \quad (\text{A7})$$

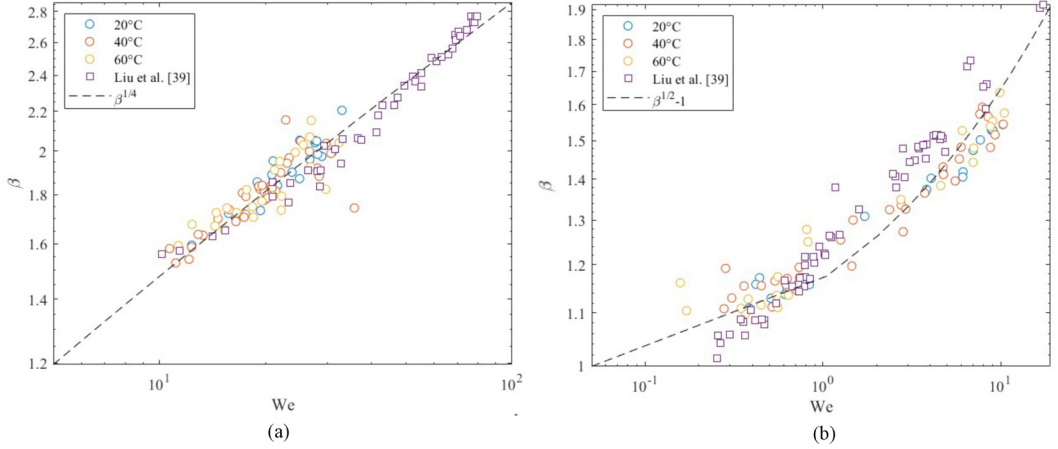


FIG. 9. Comparison of our experiment results in different temperatures, previous study's results, and the predicted model. The law appears to be the same.

Adopting the perturbation method for an approximate solution, we can obtain

$$\frac{2a}{D_0} - 1 = 6 \text{Bo} \propto \text{Bo}. \quad (\text{A8})$$

Furthermore, through experimental fitting, it was observed that the spreading coefficient  $\beta$  is related to  $\frac{2a}{D_0} - 1$ :

$$\beta \propto \left( \frac{2a}{D_0} - 1 \right)^{0.40}. \quad (\text{A9})$$

By comparing  $\text{We}^{1/2}$  (ignoring the gravity limit) with  $\text{Bo}$  (ignoring the kinetic energy limit) and using Padé approximation [42], we ultimately obtain the relationship satisfied by the spreading coefficient:

$$\beta \propto \left( \text{We}^{1/2} + \frac{\text{Bo}}{A} \right)^{0.40}. \quad (\text{A10})$$

However, within the scope of this experiment,  $\text{Bo}$  has a negligible impact on the final fitting results. Therefore, we further simplify the relationship to

$$\beta \propto \text{We}^{1/2}. \quad (\text{A11})$$

We apply this conclusion to our experimental data, and the theoretical and experimental results match well (demonstrated in the updated theoretical graph in Fig. 9). In this derivation, we did not impose any requirements on surface properties but solely considered the parameters and shape characteristics of the droplet itself. Therefore, the theory is also universally applicable. At this point, we have obtained the maximum spreading law of droplets on dry ice surfaces. Next, we will investigate the law governing their rebound time.

## APPENDIX B: THE CONTACT TIME

The measured rebound time corresponding to the time points is shown in Fig. 7. Regarding the theoretical modeling of droplet rebound time, whether it is the elastic model by Richard *et al.* [4] or the water spring model by Okumura *et al.* [5], the droplet's rebound time is only related to its own deformation properties. Therefore, as long as the droplet's shape change during rebound matches



their studies, their theories can be applicable. From the experimental observations of Antonini and our own, it is evident that the shape change of droplets rebounding on dry ice is indeed similar to that on superhydrophobic surfaces. Thus, the rebound time law for droplets on superhydrophobic surfaces can be applied to dry ice surfaces. To obtain the quantitative law for the rebound time of droplets on dry ice surfaces, we consider the Euler equation for liquid deformation:

$$\rho \frac{Dv}{Dt} = -\nabla p + \rho g, \quad (\text{B1})$$

where  $t \propto \frac{x}{v}$ , and according to the Lagrange surface tension formula,  $P \propto \frac{\sigma}{R_0(1 \pm \frac{\sigma}{\rho R_0^2})}$ , which implies  $\nabla p \propto \frac{\sigma x}{R_0^3}$ . Thus, we obtain

$$\rho v^2 R_0^3 \propto \sigma x^3 - \rho g R_0^3 x. \quad (\text{B2})$$

If we neglect the influence of gravity,  $x \propto \sqrt{\frac{\rho R_0^3}{\sigma}} v$ . Therefore,

$$t \propto \frac{x}{v} \propto \sqrt{\frac{\rho R_0^3}{\sigma}}. \quad (\text{B3})$$

If we consider the influence of gravity, the equation can be written as

$$\rho v^2 R_0^3 + \sigma \delta^2 \propto \sigma (x - \delta)^2. \quad (\text{B4})$$

We can consider this as an energy equation for a spring model with an initial displacement  $\delta$ ; thus, its period remains unchanged, indicating

$$t \propto \frac{x}{v} \propto \sqrt{\frac{\rho R_0^3}{\sigma}}. \quad (\text{B5})$$

We compare this theoretical derivation with experimental data and find a good agreement. Furthermore, based on experimental data, we perform a fitting process for the coefficients in the previous equation, yielding the specific formula as follows (in Fig. 10):

$$\tau = 2.6 \sqrt{\frac{\rho R_0^3}{\sigma}}. \quad (\text{B6})$$

Furthermore, due to the droplet's Ohnesorge number (Oh) being  $\ll 1$ , we neglect the internal viscous forces within the droplet. We only consider inertial forces and surface tension. Therefore, according to the previously established theoretical model, water droplets and alcohol droplets should exhibit the same spreading coefficient and rebound time patterns.

In addition, we have conducted the same experiment above in different temperatures and the results have already been included in the figure above which shows the consistency of the phenomenon in different temperatures, so the conclusion above can also be used in different temperature situations.

### APPENDIX C: HEAT TRANSFER DURING THE REBOUND PROCESS

We simplified the heat transfer of the droplet and dry ice surface as a one-dimensional unsteady-state heat conduction equation. The control equation is as follows:

$$\frac{\partial t}{\partial \tau} = a \frac{\partial^2 t}{\partial x^2}. \quad (\text{C1})$$

$t$  is the temperature,  $\tau$  is the time, and  $a = \frac{k}{c}$ , where  $k$  is the heat conductivity and  $c$  is the specific heat. The initial condition is that  $t = 293$  K when  $\tau = 0$ ,  $t = 201$  K when  $x = 0$ , and when  $x \rightarrow \infty$ ,

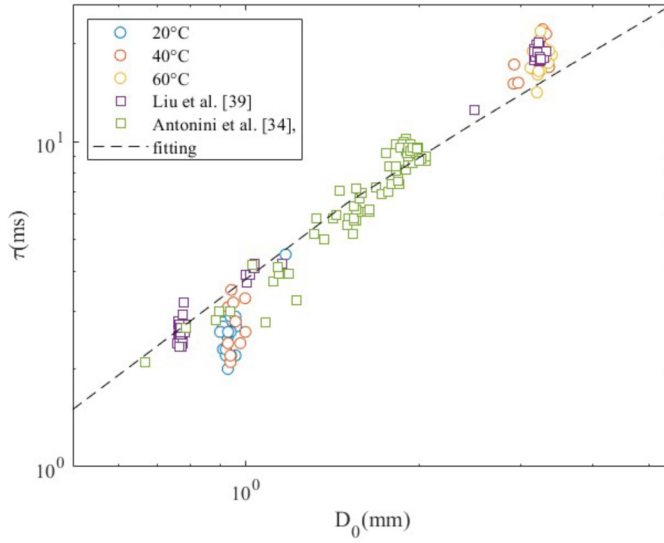


FIG. 10. The rebound time of droplets in different temperatures in our experiment yields similar results to previous studies (data sourced from Liu *et al.* [41] and Antonini *et al.* [34]).

$t = 293$  K. The analytical solution of the equation is given by  $\frac{t-293}{201-293} = 1 - \operatorname{erf}\left(\frac{x}{2\sqrt{a\tau}}\right)$ , where  $\operatorname{erf}(u) = \frac{2}{\sqrt{\pi}} \int_0^u e^{-x^2} dx$  is the Gaussian error function and its value can be checked in tables. When  $u = 2$ ,  $1 - \operatorname{erf}(u) = 0.00047 \approx 0$ , so we can consider that when it's the time  $\tau$ , the temperature of the place  $x = 4\sqrt{a\tau}$  has not changed. This  $x$  is called penetration depth. Then we calculate its heat flux density.

$$q = -k \frac{\partial t}{\partial x} = k \frac{92 \text{ K}}{\sqrt{\pi a \tau}}. \quad (\text{C2})$$

The heat transfer in time  $\tau$  is  $Q = \int_0^\tau q d\tau$ . We substitute the specific data into the equation. The contact time is taken as 10 ms according to our experiment. The penetration depth  $x = 0.15$  mm and the heat transfer  $Q = 16519 \text{ J/m}^2$ . So the average temperature drop of the liquid within this depth will reach 26.22 K while the droplets' origin temperature is 293 K. Moreover, the temperature of the portion closer to the surface will be even lower. Hence, the bottom of the droplet will freeze once the droplet comes into contact with the dry ice surface.

- 
- [1] C. Clanet, C. Béguin, D. Richard *et al.*, Maximal deformation of an impacting drop, *J. Fluid Mech.* **517**, 199 (2004).
  - [2] N. Laan, Maximum diameter of impacting liquid droplets, *Phys. Rev. Appl.* **2**, 044018 (2014).
  - [3] X. Yu, Water droplet bouncing dynamics, *Nano Energy* **81**, 105647 (2021).
  - [4] D. Richard, C. Clanet, and D. Quere, Contact time of a bouncing drop, *Nature (London)* **417**, 811 (2002).
  - [5] K. Okumura, Water spring: A model for bouncing drops, *Europhys. Lett.* **62**, 237 (2003).
  - [6] T.-S. Wong, Bioinspired self-repairing slippery surfaces with pressure-stable omniphobicity, *Nature (London)* **477**, 443 (2011).
  - [7] C. Chen, Cauliflower-like micro-nano structured superhydrophobic surfaces for durable anti-icing and photothermal de-icing, *Chem. Eng. J.* **450**, 137936 (2022).

- [8] R. Rioboo, C. Bauthier, J. Conti, Experimental investigation of splash and crown formation during single drop impact on wetted surfaces, *Exp. Fluids* **35**, 648 (2003).
- [9] S. T. Thoroddsen and J. Sakakibara, Evolution of the fingering pattern of an impacting drop, *Phys. Fluids* **10**, 1359 (1998).
- [10] F. H. Harlow and J. P. Shannon, The splash of a liquid drop, *J. Appl. Phys.* **38**, 3855 (1967).
- [11] M. Pasandideh-Fard, S. D. Aziz, S. Chandra, Cooling effectiveness of a water drop impinging on a hot surface, *Int. J. Heat Fluid Flow* **22**, 201 (2001).
- [12] B. Bhushan, Y. C. Jung, and K. Koch, Micro-, nano- and hierarchical structures for superhydrophobicity, self-cleaning and low adhesion, *Philos. Trans. R. Soc. A* **367**, 1631 (2009).
- [13] A. Lafuma and D. Quéré, Superhydrophobic states, *Nat. Mater.* **2**, 457 (2003).
- [14] J. Eggers, Drop dynamics after impact on a solid wall: Theory and simulations, *Phys. Fluids* **22**, 062101 (2010).
- [15] T. Bennett and D. Poulikakos, Splat-quench solidification: Estimating the maximum spreading of a droplet impacting a solid surface, *J. Mater. Sci.* **28**, 963 (1993).
- [16] M. Reyssat, A. Pépin, F. Marty, Bouncing transitions on microtextured materials, *Europhys. Lett.* **74**, 306 (2006).
- [17] D. Bartolo, F. Bouamrène, E. Verneuil, Bouncing or sticky droplets: Impalement transitions on superhydrophobic micropatterned surfaces, *Europhys. Lett.* **74**, 299 (2006).
- [18] D. Richard and D. Quéré, Bouncing water drops, *Europhys. Lett.* **50**, 769 (2000).
- [19] L. Chen, Z. Xiao, P. C. H. Chan, A comparative study of droplet impact dynamics on a dual-scaled superhydrophobic surface and lotus leaf, *Appl. Surf. Sci.* **257**, 8857 (2011).
- [20] A. I. Aria and M. Gharib, Physicochemical characteristics and droplet impact dynamics of superhydrophobic carbon nanotube arrays, *Langmuir* **30**, 6780 (2014).
- [21] X. Wang, Y. B. Wang, L. L. Jiao, Energy analysis on rebound dynamics of two droplets impacting a superhydrophobic surface simultaneously, *AIP Adv.* **11**, 055007 (2021).
- [22] A. L. Biance, C. Clanet, and D. Quéré, Leidenfrost drops, *Phys. Fluids* **15**, 1632 (2003).
- [23] J. G. Leidenfrost, *De Aquae Communis Nonnullis Qualitatibus Tractatus* (Ovenius, Duisburg ad Rhenum, 1756).
- [24] D. Quéré, Leidenfrost dynamics, *Annu. Rev. Fluid Mech.* **45**, 197 (2013).
- [25] C. Cai, H. Liu, H. Chen, Alcohol-induced elevation in the dynamic Leidenfrost point temperature for water droplet impact, *Int. J. Heat Mass Transfer* **215**, 124483 (2023).
- [26] J. C. Burton, A. L. Sharpe, R. C. A. Van Der Veen, Geometry of the vapor layer under a Leidenfrost drop, *Phys. Rev. Lett.* **109**, 074301 (2012).
- [27] T. Tran, H. J. J. Staat, A. Prosperetti, Drop impact on superheated surfaces, *Phys. Rev. Lett.* **108**, 036101 (2012).
- [28] M. Jiang, Y. Wang, F. Liu, Inhibiting the Leidenfrost effect above 1,000 °C for sustained thermal cooling, *Nature (London)* **601**, 568 (2022).
- [29] M. Mrinal, X. Wang, and C. Luo, Self-rotation-induced propulsion of a Leidenfrost drop on a ratchet, *Langmuir* **33**, 6307 (2017).
- [30] S. Hidalgo-Caballero, Y. Escobar-Ortega, and F. Pacheco-Vázquez, Leidenfrost phenomenon on conical surfaces, *Phys. Rev. Fluids* **1**, 051902 (2016).
- [31] M. He, H. Li, J. Wang, Superhydrophobic surface at low surface temperature, *Appl. Phys. Lett.* **98**, 093118 (2011).
- [32] Y. S. Song, D. Adler, F. Xu, Vitrification and levitation of a liquid droplet on liquid nitrogen, *Proc. Natl. Acad. Sci. USA* **107**, 4596 (2010).
- [33] M. Adda-Bedia, S. Kumar, F. Lechenault, Inverse Leidenfrost effect: Levitating drops on liquid nitrogen, *Langmuir* **32**, 4179 (2016).
- [34] C. Antonini, I. Bernagozzi, S. Jung, Water drops dancing on ice: How sublimation leads to drop rebound, *Phys. Rev. Lett.* **111**, 014501 (2013).
- [35] A. Milionis, C. Antonini, S. Jung, Contactless transport and mixing of liquids on self-sustained sublimating coatings, *Langmuir* **33**, 1799 (2017).

- [36] A. Muginstein, M. Fichman, and C. Gutfinger, Gas absorption in a moving drop containing suspended solids, *Int. J. Multiphase Flow* **27**, 1079 (2001).
- [37] M. Schremb, I. V. Roisman, and C. Tropea, Transient effects in ice nucleation of a water drop impacting onto a cold substrate, *Phys. Rev. E* **95**, 022805 (2017).
- [38] Z. Jin, H. Zhang, and Z. Yang, Experimental investigation of the impact and freezing processes of a water droplet on an ice surface, *Int. J. Heat Mass Transfer* **109**, 716 (2017).
- [39] J. Li and P. B. Weisensee, Low Weber number droplet impact on heated hydrophobic surfaces, *Exp. Therm. Fluid Sci.* **130**, 110503 (2022).
- [40] I. S. Khattab, F. Bandarkar, M. A. A. Fakhree, Density, viscosity, and surface tension of water+ethanol mixtures from 293 to 323K, *Korean J. Chem. Eng.* **29**, 812 (2012).
- [41] Y. Liu, Y. Liu, and M. Chen, Maximum spreading diameter of bouncing droplets at ultralow Weber numbers, *Langmuir* **39**, 7922 (2023).
- [42] W. H. Press, *Numerical Recipes 3rd Edition: The Art of Scientific Computing* (Cambridge University Press, 2007).